Online Identification and Detection of Manual Control Adaptation with Recursive Time Series

Plaetinck, Wouter; Pool, D.M.; van Paassen, M.M.; Mulder, Max

DOI
10.2514/1.G007980

Publication date
2025

Document Version
Final published version

Published in
Journal of Guidance, Control, and Dynamics: devoted to the technology of dynamics and control

Citation (APA)
Plaetinck, W., Pool, D. M., van Paassen, M. M., & Mulder, M. (2025). Online Identification and Detection of Manual Control Adaptation with Recursive Time Series. *Journal of Guidance, Control, and Dynamics: devoted to the technology of dynamics and control*, *48*(5), 1112-1123. https://doi.org/10.2514/1.G007980

JOURNAL OF GUIDANCE, CONTROL, AND DYNAMICS
Vol. 48, No. 5, May 2025

Online Identification and Detection of Manual Control Adaptation with Recursive Time Series

Wouter Plaetinck,* Daan M. Pool,† Marinus M. van Paassen,‡ and Max Mulder§
Delft University of Technology, 2600 GB Delft, The Netherlands

https://doi.org/10.2514/1.G007980

An online pilot manual control behavior identification method, based on recursive low-order time-series model estimation, is presented and validated using experimental data. Eight participants performed compensatory tracking tasks with time-varying vehicle dynamics, where, at an unpredictable moment during a run, a sudden degradation in dynamics could occur. They were instructed to push a button when they detected a change in dynamics. Two methods to automatically detect the moment when pilot adaptation occurs from online estimated parameter traces are discussed. Results show that pilots are more accurate in detecting changes than either algorithm. But when the algorithms are correct, they are often quicker to detect pilot adaptation than pilots themselves. The presented techniques have potential but need improvements.

I. Introduction

ALTHOUGH levels of automation seem ever-increasing, the majority of safety-critical systems still require the involvement of human operators (HOs), e.g., to deal with unexpected situations that can be extremely difficult to anticipate and fully automate. In aviation, pilots' capacity for quick and timely adaptation is regarded as critical to deal with changes in the vehicle dynamics caused by aircraft damage and autopilot or stabilization system mode switches or disengagement [1–3]. Systems to support pilots in dealing with these (unexpected, sudden) changes are being developed, for instance, through haptic shared control [4], in the context of aircraft loss-of-control mitigation [5].

Adaptive support systems are likely to affect the stability of the closed-loop control system and, with that, the safety of operation. The changing dynamics of both vehicle and operator must be accounted for. A first crucial enabler is therefore to detect, preferably in real time, changes in the vehicle dynamics, an active field of study since the 1970s leading to many methods to objectively measure the controlled element (CE) dynamics [5]. Our knowledge about when and how HOs adapt to changing CE dynamics, the second key enabler, is significantly lacking. Advancements since Young's seminal paper on adaptive manual control [6] have been small.

Techniques to estimate changes in pilot dynamics form a niche in the domain of system identification and are much less successful than methods that estimate steady-state HO behavior. Human controllers are nonlinear, noisy, and time-varying; their dynamics need to be estimated in closed loop; and in many real-life control situations, the human *inputs* are unknown [7]. In aircraft control, for instance, the pilot's brain and body can close a plethora of loops using visual and vestibular inputs, patterns that all potentially relate to the pilot's output, which is known. Manual control studies describe human control behavior in situations where the task variables (CE dynamics, displays, manipulators) are constant [8–10]. The resulting objective, quantitative modeling approaches mainly consider HOs as (quasi-) linear, time-invariant (LTI) feedback systems [11–13].

To investigate time-varying HO behavior, this time-invariance assumption must be abandoned [12]. There is a need to be able to detect *when* an operator adapts and to model *how* this adaptation is performed in real time. Not only would this ability be extremely useful from a scientific perspective, it would also allow for many novel applications. Examples are the adaptive operator support systems mentioned above but also systems to detect reduced operator attention or distraction and fatigue [14]. These all need an online operator monitoring component to work.

Two main techniques for capturing time-varying pilot behavior were developed in previous work. Time-varying behavior was either captured in empirically derived logic rules [1,15] or determined using system identification methods. Studies taking the second perspective tried to identify human adaptation to time-varying CE dynamics [2] and other time-varying task variables such as visual [16] and physical motion [17] and control manipulator changes [18]. These studies mostly aimed at offline, a posteriori, identification and can be classified to fit either a batch of data at once or to estimate model parameters recursively. All applied different ways of introducing the adaptation in the operator model. For example, in [19] wavelets were applied. Zaal [2] used genetic maximum likelihood estimation while the adaptation is assumed to follow a sigmoid shape, the defining parameters of which are included in the estimation. In [20] a linear parameter-varying model is fit with experimentally determined scheduling functions to represent the adaptation. In [21] a two-step method is used: the wavelet transform identifies a time-varying frequency response, and then an operator model is fit to that response. All are batch estimation methods and thus not directly applicable online [22].

Recursive methods require no assumption on the shape (or time) of adaptation and are directly applicable for online estimation. A nonparametric method combines finite impulse response estimation with recursive least squares (RLS) [18]. Parametric methods include the extended Kalman filter [16,23], dual extended Kalman filter [24], and unscented Kalman filter [25] to estimate the HO parameters directly. Alternatively, autoregressive with exogenous (ARX) input models can be used with an RLS estimation of the ARX model coefficients, which are then converted to HO parameters [26]. The authors of Ref. [26] extend existing LTI techniques to time-varying HO modeling [27,28].

In the state-of-the-art, a validated online HO identification method, together with a tested algorithm for detecting the moment of adaptation using estimated HO parameter traces, is missing. This paper addresses this issue, with a focus on adaptation to time-varying CE dynamics [29,30]. In Sec. II, the control task, identification, and adaptation detection methods are briefly introduced. Section III discusses the experiment conducted to test the techniques. Results are

Received 29 September 2023; accepted for publication 24 November 2024; published online 17 January 2025.

*M.Sc., Faculty of Aerospace Engineering; wouterplaetinck@hotmail.com.

†Assistant Professor, Control and Simulation, Faculty of Aerospace Engineering; d.m.pool@tudelft.nl. Associate Fellow AIAA.

‡Associate Professor, Control and Simulation, Faculty of Aerospace Engineering; m.m.vanpaassen@tudelft.nl.

§Professor, Control and Simulation, Faculty of Aerospace Engineering; m.mulder@tudelft.nl. Associate Fellow AIAA (Corresponding Author).

shown in Sec. IV and discussed in Sec. V. Conclusions are drawn in Sec. VI.

II. Methods

A. Control Task and Pilot Model

A single-axis, single-channel compensatory tracking task was set up to evaluate the HO identification and adaptation detection methods, similar to Zaal's experiment [2]. Figure 1 illustrates the task, where the HO controls the CE dynamics H_c such that its output y tracks the target forcing function f_t as closely as possible. The only feedback to the HO is the tracking error e, shown on a compensatory display. The HO provides a single control output u. In this paper, we focus on what Young [6] refers to as "controlled element adaptation," illustrated by the gray arrow in Fig. 1.

Two factors play a role in inducing time-varying HO behavior: i) the extent to which the CE dynamics change, and ii) the time it takes for the CE dynamics to change. Larger changes in dynamics that occur rapidly can be expected to be easier for pilots to detect than subtle changes that occur slowly. Whereas from an operational point of view, the latter, subtle changes, are more relevant, from an experimental perspective, the former, rapid changes, are preferred, as then the chance of detection increases. To align with other recent experiments on time-varying HO behavior [2,24,25], we adopted Zaal's approach [2016], who changed the CE dynamics in Eq. (1) over time according to a sigmoid scheduling function (2).

$$H_c(s,t) = \frac{K_c(t)}{s^2 + \omega_c(t)s} \tag{1}$$

$$P(t) = P_1 + \frac{P_2 - P_1}{1 + e^{-G(t-M)}} \tag{2}$$

In Eq. (2) the P_1 and P_2 parameters describe the initial and final values of the sigmoid function $P(t)$, respectively. Both the CE gain K_c and break frequency ω_c of Eq. (1) were scheduled, substituting the initial value P_1 and final value P_2 for the respective CE parameter values.

The sigmoid transition is characterized by a maximum rate of change G and centered around time M, the "moment of transition." Assuming a measurement run to last $T_m = 81.92$ s and putting M half-way the run, the transition in the CE parameters is illustrated in Fig. 2 for two settings of G. In the fast ($G = 100$ s^{-1}) and slow ($G = 0.5$) settings the system dynamics change in approximately

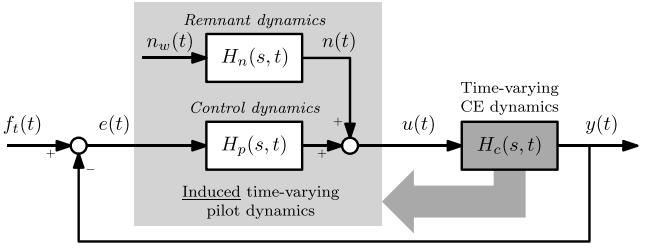

Fig. 1 A compensatory tracking task with time-varying CE dynamics and adapting quasi-linear HO model.

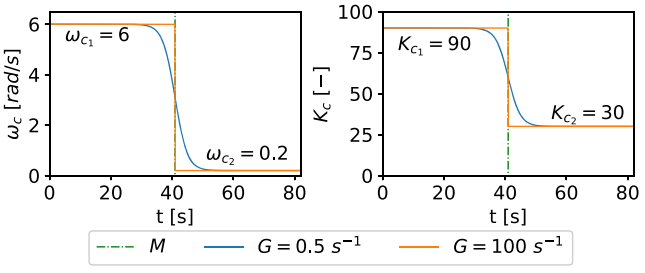

Fig. 2 CE parameters scheduled by sigmoid function for fast ($G = 100$ s^{-1}) and slow change ($G = 0.5$ s^{-1}).

0.35 and 15 s, respectively. Whereas the initial CE dynamics resemble single-integrator-like dynamics in the crossover region, the final CE dynamics approximate a double integrator in the crossover region, *forcing* the HO to generate lead to stabilize the system [8]. It is this necessary change in HO lead that we hypothesize to be detectable by our methods and also causes the HO to detect the CE variation.

A validated HO model in time-invariant compensatory control tasks is McRuer's simplified precision model, a quasi-linear model [8]. It consists of a linear time-invariant describing function $H_p(s)$ and an additive noise, called remnant, with filter $H_n(s)$, as in Fig. 1. The remnant n is used to describe nonlinear, randomly time-varying effects in HO behavior [8]. A common describing function $H_p(s)$ for the considered CE dynamics is:

$$H_p(s) = K_e(1 + T_L s)e^{-s\tau}H_{nm}(s) \tag{3}$$

where $H_{nm}(s)$ represents the neuromuscular dynamics, and K_e, T_L and τ are the HO gain, lead time (in seconds), and effective time delay (in seconds), respectively. The possibly also time-varying neuromuscular system (NMS) dynamics are modelled as a second-order system with natural frequency ω_{nm} in rad/s and damping ratio ζ_{nm} [31]:

$$H_{nm}(s,t) = \frac{\omega_{nm}^2(t)}{\omega_{nm}^2(t) + 2\zeta_{nm}(t)\omega_{nm}(t)s + s^2} \tag{4}$$

The NMS dynamics were included in the model because the forcing functions applied in the experiment (Sec. III) excited our participants' control dynamics also at higher frequencies, where the NMS dynamics dominate. Our high-performance experimental setup allows for these NMS dynamics to be estimated. Excluding the NMS dynamics would mean that the ARX time series model (discussed next) would not be able to capture the measured HO behavior with sufficient accuracy to facilitate reliable detection of behavior/parameter changes.

To model the time-varying HO, it was assumed that the describing function in Eq. (3) still holds if all its parameters are free to vary over time. To reduce a possible identification ambiguity between the HO error response gain K_e and lead time constant T_L, an explicit error rate response gain $K_{\dot{e}}(t) = K_e(t)T_L(t)$ was introduced:

$$H_p(s,t) = (K_e(t) + K_{\dot{e}}(t)s)e^{-s\tau}H_{nm}(s,t) \tag{5}$$

Due to identification method constraints (discussed later), the HO delay τ was assumed constant, which was found valid for the considered task in earlier work reported by Zaal [2]. Summarizing, the HO model used in this paper has four time-varying parameters $(K_e, K_{\dot{e}}, \omega_{nm}, \zeta_{nm})$ and one time-invariant parameter (τ) to be estimated.

B. Online Time-Varying HO Model Identification Using ARX

Using measured time traces of the tracking error e and control signal u, a model for the HO can be identified. In this paper, an "autoregressive exogenous" (ARX) model structure is used for this purpose [26]. The ARX coefficients are first obtained using RLS and then converted to the actual HO model parameters to complete the identification process. The method is explained in detail in [26,30] and will be summarized below.

1. *ARX Model Structure*

The general ARX model structure is shown in Eq. (6). This is a discrete-time model with time shift operator q, such that $q^{-n_k}e(t) = e(t - n_k)$ models the HO delay. The HO describing function is approximated by the ratio $B(q)/A(q)$ and delay shift of n_k samples. In ARX models, the HO remnant noise is modeled by the ratio $1/A(q)$, which filters a white noise input signal $\epsilon(t)$. Note that the process and noise dynamics are thus coupled through $A(q)$, potentially leading to biased estimates, depending on the power and spectrum of the remnant signal [26]:

$$u(t) = \frac{B(q)}{A(q)} q^{-n_k} e(t) + \frac{1}{A(q)} \epsilon(t) \tag{6}$$

Second-order $A(q)$ and $B(q)$ polynomials were chosen to match Eq. (5) and to allow for a straightforward HO parameter retrieval, as described later. This results in Eq. (7) for the HO model approximation $H_p(q)$. The model structure allows the use of RLS for the polynomial coefficients but not for the time shift parameter n_k [26], which was assumed to be set *a priori* at 28 corresponding to $\tau = 0.28$ s [2] (simulation running at 100 Hz; time step $\Delta t = 0.01$ s).

$$H_p(q) = \frac{B(q)}{A(q)} q^{-n_k} = \frac{b_0^d + b_1^d q^{-1}}{1 + a_1^d q^{-1} + a_2^d q^{-2}} q^{-n_k} \tag{7}$$

Preliminary attempts to include n_k in the (potentially online) estimation are described in [29]. Batch ARX results of n_k estimates are reported in [26]. Both attempts only used simulated HO behavior and showed that estimating n_k is challenging. The work of Zaal [2], featuring the same CE dynamics and forcing function used here, showed that the value $\tau = 0.28\ s$ is representative for the HO delay found when controlling systems transitioning from single-integrator-like to double-integrator-like dynamics. Applying McRuer's "Verbal Adjustment Rules" [8] for CEs in between pure integrator and pure double-integrator dynamics, a time delay of 0.28 s would correspond with tracking a forcing function f_t with a bandwidth of 2.3 rad/s, close to the current task (1.3 rad/s; see Sec. III.B).

2. *Recursive Least Squares and HO Parameter Retrieval*

The ARX model can be rewritten in linear regression form as $\hat{u}[i|i-1, \theta_i] = \varphi[i]\theta_i$, for each step i, with the regression vector φ and coefficient vector θ_i in Eqs. (8) and (9); see [32].

$$\varphi[i] = \begin{pmatrix} -u[i-1] & -u[i-2] & e[i-n_k] & e[i-n_k-1] \end{pmatrix} \tag{8}$$

$$\theta_i = \begin{pmatrix} a_1^d & a_2^d & b_0^d & b_1^d \end{pmatrix}^T \tag{9}$$

An RLS algorithm with exponential forgetting factor λ (here set at 0.99609 based on previous work [26]) was used to estimate the ARX coefficients, (9). These were then converted to the four continuous-time time-varying HO describing function parameters ($K_e, K_{\dot{e}}, \omega_{nm}, \zeta_{nm}$). The ARX model can be written as a discrete-time transfer function $H_p(z)$ using the following Z-transform property: $Z[q^{-n} f(i\Delta t)] = z^{-n} F(z)$. Note that $n_k = \tau/\Delta t$ in Eq. (10).

$$H_p(z) = \frac{b_0^d + b_1^d z^{-1}}{1 + a_1^d z^{-1} + a_2^d z^{-2}} z^{-\frac{\tau}{\Delta t}} \tag{10}$$

The estimate for this discrete-time transfer function will be updated at each time step. To retrieve the HO model parameters, it needs to be converted to its continuous-time equivalent. Using a zero-order-hold conversion yields:

$$H_p(s) = \frac{b_0^c s + b_1^c}{s^2 + a_1^c s + a_2^c} e^{-s\tau} \tag{11}$$

Comparing Eq. (11) with the HO model in Eqs. (4) and (5), the following relations are then obtained:

$$\begin{aligned} K_e &= \frac{b_1^c}{a_2^c} & K_{\dot{e}} &= \frac{b_0^c}{a_2^c} \\ \zeta_{nm} &= \frac{a_1^c}{2\sqrt{a_2^c}} & \omega_{nm} &= \sqrt{a_2^c} \end{aligned} \tag{12}$$

When using higher-order ARX models, these relations between the ARX coefficients and the HO model parameters become overdetermined, and a model order reduction technique is required [26,32].

3. *Estimation Biases*

Van Grootheest et al. [26] reported on the potential biases in the estimated parameters using the recursive ARX method. The estimated control dynamics and remnant dynamics are coupled in the $A(q)$ polynomial for ARX models, resulting in biased estimates proportional to the remnant level. Different models for the remnant can mitigate these effects [26]. Different model structures (such as autoregressive moving average with exogenous (ARMAX) inputs or Box–Jenkins models [32]) may also mitigate these issues. As these model structures are currently, to the best of our knowledge, not applicable in real time, the ARX model structure is maintained.

C. Automatic HO Adaptation Detection

For the considered task, with the CE dynamics changing from integrator-like to double-integrator-like dynamics, the expected HO adaptation is a reduced error gain K_e and increased error rate gain $K_{\dot{e}}$: more lead compensation is required [8]. For the considered change in CE dynamics, the delay and neuromuscular parameters were found not to vary significantly in the experiments of Zaal [2]. With the HO delay assumed constant, the adaptation detection methods will need to be based on time traces of either K_e or $K_{\dot{e}}$ estimates, where the largest changes are expected to occur.

1. *Two Methods: TICA and MA*

Two detection methods are proposed, and both use an "average measure" of the considered estimated parameter, plus or minus a certain margin, i.e., the "reference band." Figures 3a and 3b illustrate the working principle, for $K_{\dot{e}}$ only; K_e is equivalent. The used time-varying average measure is method-specific, as will be described below. The width of the reference band (blue area) is set by the $\delta K_{\dots}$ value, a hyperparameter that is the same for both methods.

The two methods differ in what time-varying average measure is used for the reference band. First, in the time-invariant condition average (TICA) method, the average measure is calculated by averaging the identified time-varying ARX parameter estimate traces of the three *a priori* measured time-invariant task runs, in which the HO controlled the initial single-integrator-like CE dynamics (Fig. 2). For every participant, an average trace was stored, which contained small time variations as are clear in Fig. 3a. Second, in the moving average (MA) method, the average measure is calculated through applying a moving average, over a window of n_s samples up to the current step i, of the identified parameter trace in that run. See Eq. (13) for $K_{\dot{e}}$; the calculation for K_e is equivalent:

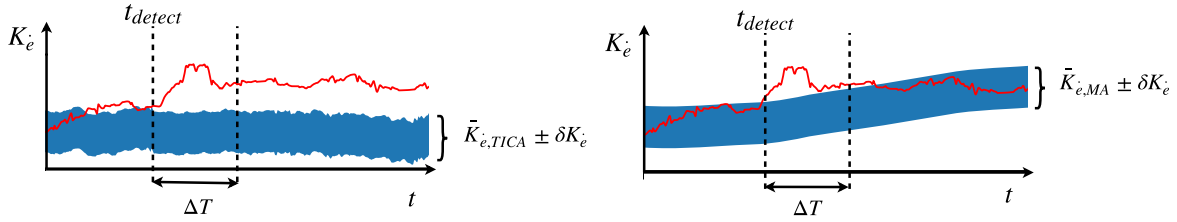

a) TICA method **b) MA method**

Fig. 3 Illustration of adaptation detection for a) TICA and b) MA methods.

$$K_{\dot{e},\mathrm{MA}} = \frac{1}{n_s}\sum_{k=0}^{n_s-1} K_{\dot{e}_{i-k}} \tag{13}$$

For every participant, the actual, but smoothed, average trace is obtained (see Fig. 3b).

Both methods were applied to identified traces of both K_e and $K_{\dot{e}}$. In Figs. 3a and 3b the reference band (blue) represents the nonadapted HO behavior (TICA) or adapting HO behavior (MA), with a margin for typical oscillations seen in the estimated parameter value (red trace). When the estimated parameter moves outside this band at a particular time and remains outside this band for a period longer than a window with length ΔT, in seconds, an adaptation is considered "detected," and the initial time of the current window saved as t_{detect}, further referred to as t_d.

2. *Hyperparameter Tuning*

To minimize false positives (FPs) and false negatives (FNs), both methods require hyperparameter tuning. An FP would occur when a detection was made outside the interval $M < t_d < 60$ s, with $M = 40.96$ s the central moment of transition; see Eq. (2). The limit of 60 s was arbitrarily chosen, since by then HOs should have adapted to the new CE dynamics (if not, the loop would become unstable) and the estimated parameters should be sufficiently converged to trigger a detection. An FN would occur when no detection was made. This, for instance, can happen when the parameter trace did not go outside the reference band for longer than ΔT seconds during a run.

The following hyperparameters are tuned. For both methods, the accepted variability margin parameters δK_e and $\delta K_{\dot{e}}$ define the width of the reference band (around the middle defined above) that sets the allowed (or expected) deviation of the HO parameter estimates from the average. For both methods, ΔT sets the minimum time the estimated parameter trace should be outside the reference band for the parameter deviation to be considered a detection. For the MA method, n_s defines the number of samples taken in the moving average calculation [Eq. (13)]; hence, this parameter directly affects the MA method's tracking speed.

A sensitivity study of the detection performance with respect to the described hyperparameters will be performed for each method (Sec. IV). Each hyperparameter will be varied over a relevant range while keeping the other hyperparameters at their initial chosen value. Parameters λ (forgetting factor) and n_k (HO time delay) will remain fixed. For each combination of variability margin, ΔT and n_s (MA only), the mean-squared error (MSE) of the estimated detection time t_d with respect to the actual (central) moment of transition M can be calculated:

$$\mathrm{MSE}(\delta K_{\dot{e}}, \Delta T, n_s) = \frac{1}{n_{\mathrm{runs}}}\sum_{j=1}^{n_{\mathrm{runs}}} (M - t_d[j; \delta K_{\dot{e}}, \Delta T, n_s])^2 \tag{14}$$

In Eq. (14), the MSE calculation is shown for $K_{\dot{e}}$; it is equivalent for K_e. This will be repeated for all measured runs in a certain condition. In case of a too early detection ($t_d < M$) or no detection, the maximum possible MSE will be assigned for that run by setting $t_d = 0$ s. TICA will be used as a baseline, as for most applications a priori knowledge of parameter variations in equivalent time-invariant scenarios is not available. The MA approach requires less additional data to tune and is therefore more promising for online implementation.

III. Experiment Setup

An experiment was done to evaluate the performance of the online recursive ARX identification to tune and evaluate the TICA and MA detection methods. Adaptation detection times *as experienced by the HOs* were also obtained.

A. Apparatus

The experiment was performed in the fixed-base Human-Machine Interaction Laboratory (HMI lab). Task simulation and identification modules ran at 100 Hz. The control task was an aircraft pitch attitude compensatory tracking task (Fig. 1). Participants were seated approximately 75 cm in front of a simplified artificial horizon display, as in Fig. 4b, showing the pitch tracking error e between the aircraft symbol and the horizon line. The display had an update rate of 60 Hz, and the display lag for this setup was determined to be 20–25 ms.

Control inputs were given with an electrohydraulic side-stick at the participant's right-hand side, as in Fig. 4a. The stick's torsional stiffness was 2.5 $(\mathrm{N}\cdot\mathrm{m})/\mathrm{rad}$, its damping 0.22 $(\mathrm{N}\cdot\mathrm{m}\cdot\mathrm{s})/\mathrm{rad}$, and its inertia 0.01 $\mathrm{kg}\cdot\mathrm{m}^2$, with a moment arm of 9 cm. The stick could only rotate around the pitch axis. A push button on the stick (see Fig. 4c) was used by the participants to indicate when they detected a change in the CE.

On the researcher's monitoring station (not shown), the tracking performance (root-mean-squared error, RMS(e)), time-varying HO model parameter estimation results, and the adaptation detection (button push) by the participant could be monitored in real time throughout the experiment.

B. Forcing Function

The forcing function f_t was defined as a sum of 10 sinusoids with different frequencies, amplitudes, and phases as in Eq. (15). The frequencies were integer multiples of the base measurement frequency $\omega_m = 2\pi/T_m$.

$$f_t(t) = \sum_{k=1}^{10} A_f[k]\sin(n_f[k]\omega_m t + \phi_f[k]) \tag{15}$$

This forcing function, Table 1, was identical to the signal used by Zaal [2]; it has a bandwidth of 1.25 rad/s and power 2.25 deg^2. In our experiment, f_t was shifted backward in time by 10.5 s (see Fig. 5) through adjusting the phases ϕ_f. This placed a larger magnitude change in the forcing function right within the CE dynamics transition region (see vertical line M in Fig. 5), possibly giving the HO a better chance of (early) detecting the CE transition.

C. Independent Variables

Two independent variables were manipulated: 1) the rate of change of the scheduling sigmoid for the time-varying (TV) CE dynamics G

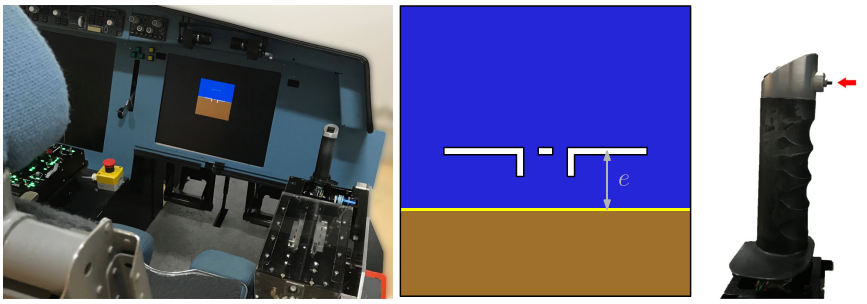

a) HMI lab simulator **b) Pitch attitude display** **c) Stick with push button**

Fig. 4 HMI lab a), compensatory display b), and control stick with push button c).

Table 1 Forcing function parameters (modified from [2]).

k	n_f	$n_f\omega_m$, rad/s	A_f, deg	ϕ_f, rad
1	3	0.230	1.186	−0.753
2	5	0.384	1.121	1.564
3	8	0.614	0.991	0.588
4	13	0.997	0.756	−0.546
5	22	1.687	0.447	0.674
6	34	2.608	0.245	−1.724
7	53	4.065	0.123	−1.963
8	86	6.596	0.061	−2.189
9	139	10.661	0.036	0.875
10	229	17.564	0.025	0.604

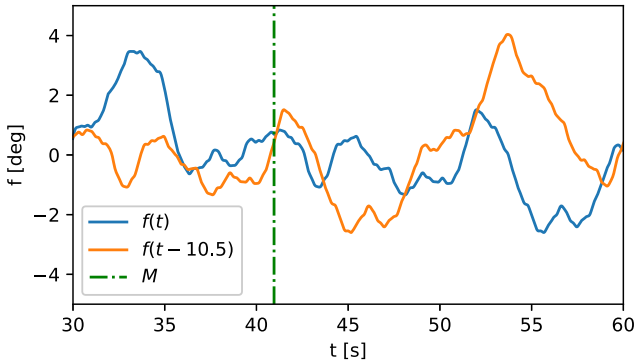

Fig. 5 View of forcing function f_t in the CE transition region (M) before and after the shift in time.

in Eq. (2) (two levels), and 2) the run-in time (three levels). In addition, two time-*invariant* (TI) reference conditions, where the CE dynamics did *not* change over time, were given to the participants. Thus, in total, eight different conditions were tested, listed in Table 2 and described below.

A transition in CE dynamics could be either present (TV) or not (TI) in a run. The time-invariant CE runs had either single-integrator-like dynamics (TI1) (H_{c_1}, with $K_c = 90, \omega_c = 6$ rad/s) or double-integrator-like dynamics (TI2) (H_{c_2}, with $K_c = 30, \omega_c = 0.2$ rad/s), the same as [2]. The estimated parameters of K_e and $K_{\dot{e}}$ in the TI1 condition were used for the "average measure" calculation in the TICA adaptation detection method (see Sec. II.C).

For runs with time-varying CE (H_{c_1} to H_{c_2}), the transition was scheduled by a sigmoid with $M = T_m/2$, thus halfway the measurement window. The maximum rate of change had two levels: $G = 0.5$ s^{-1} to represent a gradual change and $G = 100$ s^{-1} to represent an almost instantaneous change (see Fig. 2).

Each experiment run had a total measurement time of $T_m = 81.92$ s. A run-in time was added to allow possible transients, due to the HO accommodating to the task, to die out. This run-in time was varied (5, 10, and 15 s) to avoid the CE transition to become "predictable" by the participants. Care was taken to make sure that the forcing function inside the measurement window remained the same for each level and was kept aligned with M, as illustrated in Fig. 5.

Table 2 Experiment conditions.

No.	Condition	Initial CE dynamics	Final CE dynamics	Run-in time, s	G, s^{-1}
1	TI1	H_{c_1}	— —	5	— —
2	TI2	H_{c_2}	— —	5	— —
3	TV12S-T5	H_{c_1}	H_{c_2}	5	0.5
4	TV12S-T10			10	
5	TV12S-T15			15	
6	TV12F-T5			5	100
7	TV12F-T10			10	
8	TV12F-T15			15	

D. Participants, Experimental Procedure, and Instructions

Eight subjects participated, who provided written informed consent. The experiment had a training and measurement part. During training a participant performed each time-invariant condition and the two time-varying conditions, all with a run-in time of 5 s. The measurement part was divided into three blocks, with each containing the eight conditions, enabling three repeated measurements. For each block, conditions were presented in a randomized order by a balanced Latin square design. After each run, the RMS of the tracking error e was reported to motivate the participant.

Participants were instructed to maximize their tracking performance: minimize RMS(e). In addition, they were told to press the button on the stick (Fig. 4c) when they felt that the CE dynamics had changed. The time of pressing the button was recorded as t_{push}. Participants did not know whether a run contained a change in CE dynamics, and with the variation in run-in time they could also not develop a strategy (e.g., counting) to anticipate a dynamics transition.

E. Dependent Measures

Tracking performance was monitored in terms of the RMS(e) of the pitch tracking error. The discussion in this paper will focus on comparing results obtained with the subjective HO detection of the CE dynamics change, t_{push}, and the objective (TICA or MA) detection of the HO dynamics change, t_d. These two measures will be analyzed both from a numerical perspective, i.e., "how long does it take the HO to detect a change" (allowing us to calculate detection *lags*), and from the perspective of being correct or incorrect in detecting a change.

Recall from Sec. II.C.2 that the objective detection methods can be evaluated in terms of their accuracy in correctly detecting a change in the HO control behavior; the same can be done for the subjective HO detection. An FP means that the HO incorrectly pushed, in the TI1 and TI2 conditions, or pushed *before* an actual transition happened, in the six time-varying CE conditions, thus $t_{\text{push}} < M$. An FN means that the HO did not push during the run while a CE transition did in fact occur, i.e., in the time-varying conditions. True positives (TPs) indicate that the HO did push when required in those conditions; thus, $M < t_{\text{push}}$. True negatives (TNs) indicate that the HO did not push the button when it was indeed not required, as in the TI1 and TI2 conditions. Collecting all data on these decisions allows an overall detection accuracy to be calculated:

$$\text{Acc} = \frac{\text{TP} + \text{TN}}{\text{TP} + \text{FP} + \text{TN} + \text{FN}} \cdot 100\% \tag{16}$$

F. Hypotheses

Our first and main hypothesis (H.1) is that the detection in CE transitions (in case they occur) will be earlier (smaller detection lags) and more accurate (better detection performance) when the CE transition occurs faster, i.e., in the $G = 100$ s^{-1} conditions. This is because a faster CE transition will more rapidly force the HO to adapt her/his control behavior, as the system more rapidly becomes less stable.

Our secondary hypothesis (H.2) is that the run-in time variation will have no effect on the dependent measures and that all data for these variations can be lumped together. If this hypothesis is accepted, nine runs per "changing CE dynamics condition" will become available, allowing an analysis of the TV12S-T5, TV12S-T10, and TV12S-T15 data altogether as one condition, TV12S (mutatis mutandis, TV12F).

Because the detection algorithms required hyperparameter tuning, no hypotheses were stated regarding the (relative) performance of the two detection algorithms and the HO detection.

IV. Results

A. Time-Invariant Runs Parameter Estimates

Using the data from the time-invariant conditions (TI1, TI2), the five HO model parameters were estimated for each run and then averaged over the three runs per participant. Figure 6 shows boxplots

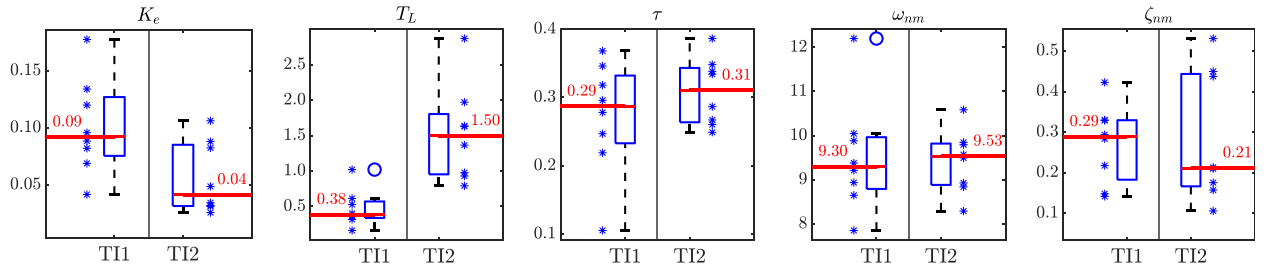

Fig. 6 Boxplots of operator model parameters for the time-invariant conditions TI1 and TI2.

of the parameter estimates. In this and later boxplots, the stars indicate individual data points (eight per condition, since we have eight subjects and averaged over three runs), the bars show the "interquartile ranges," the circles (if any) show the outliers, and the red lines and text show the medians. Figure 6 shows that the expected changes in operator behavior when comparing the single-integrator-like condition TI1 with the double-integrator-like condition TI2 indeed occur: the error gain K_e decreases, and the lead T_L increases. Similar to the experiment of Zaal [2], our results show that the operator time delay τ changes only slightly, from a median of 0.29 to 0.31 s. This also implies that fixing the operator time delay in our ARX model estimates to 0.28 s is valid, although in hindsight fixing it at 0.30 would have been better. Results of [26] indicate that biases in the estimates are small when slightly deviating from the operator delay, as done here. Note that because in both conditions lead was generated, this caused the HO time delay to change only slightly between conditions, relative to a situation where no lead would be generated, as in pure single-integrator dynamics [8]. The neuromuscular parameters remain fairly constant. In all parameters, individual differences are considerable.

B. Initial Data Processing

Using the data from the time-varying conditions, a two-way repeated-measures analysis of variance (ANOVA) was performed, with the independent variables G and run-in time as factors to check whether they affected the dependent measure t_{push}. The three repetitions with the same run-in time were first averaged per condition for each subject and then used in the ANOVA. After verifying normality and sphericity assumptions, the ANOVA revealed no significant effect on t_{push} due to run-in time ($F(2, 14) = 1.92$, $p > 0.05$), as hypothesized (H.2). The CE transition variable G did have a significant effect on t_{push} ($F(1, 7) = 15.76$, $p < 0.05$). As hypothesized (H.1), in the conditions featuring a sudden CE dynamics change

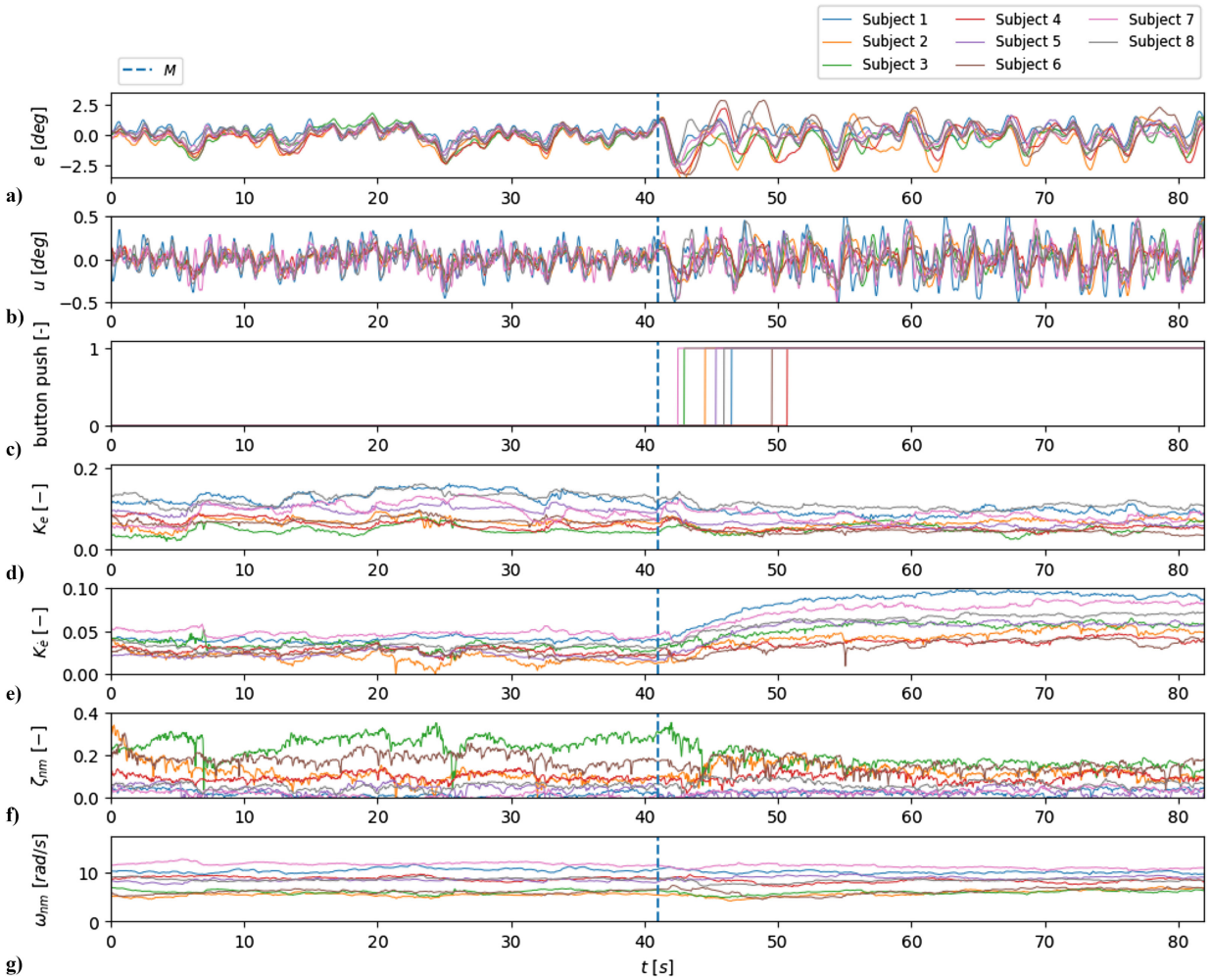

Fig. 7 Averaged time traces of control error a) and input b), median of button pushes c), and averaged time traces of identified HO parameters d–g) (all nine TV12F runs, per subject).

($G = 100\ s^{-1}$), the participants pushed the button approximately 6 s earlier than in the conditions with the gradual CE change ($G = 0.5\ s^{-1}$); this finding will be discussed further in Sec. IV.D.

This test outcome allows the trimming of the experimental data to the final 8,192 samples, corresponding to the measurement window T_m. Also, the run-in time levels can from this point on be regarded as one larger set of nine measurements (three repetitions and three run-in times) for each of the TV12S and TV12F conditions for each subject.

Two of the measurement runs (subject 2, TV12S; subject 6, TI2) were considered outliers and discarded because the RMS(e) values in these runs were more than four times higher than the average RMS(e) for these subjects. Hence, a total of 190 of the total 192 ($8 \times (6 + 9 + 9)$) measurement runs will be analyzed in the following.

To present the identification results, the parameter traces were averaged over those nine runs per time-varying condition (TV12S or TV12F) for each subject. Adaptation detection is, on the other hand, still analyzed and presented on a run-per-run basis, with condition repetitions seen as separate results.

C. Online HO Parameter Estimation

The average tracking and identified HO parameter traces per subject are shown in Figs. 7 and 8 for conditions TV12F and TV12S, respectively. In these two figures, subfigure (a) shows the operator (visual) input e, and subfigure (b) shows the operator output (stick deflection) u. Regarding tracking performance, a performance degradation (higher RMS(e), see Figs. 7a and 8a) and increase in control effort (Figs. 7b and 8b) can be seen when transitioning from the initial single-integrator-like CE dynamics to double-integrator-like dynamics, i.e., for $t > M$. This result can be expected from ample earlier experiment results (e.g., [8]).

Regarding the parameter estimate traces, a clear and expected increase in $K_{\dot{e}}$ (Figs. 7e and 8e) can be seen for all subjects in both conditions, sometimes more than 100%, showing that our participants indeed started to generate more lead when the CE dynamics changed to double-integrator-like after the moment of transition M. The expected decrease in K_e (Figs. 7d and 8d) is less evident and depends more on the subject. The neuromuscular damping noticeably decreases after the transition (Figs. 7f and 8f), which can be explained by the operator attempting to create more phase margin in the crossover region with double-integrator-like dynamics. Note that all these parameter estimates may include an unknown bias due to the unknown remnant, as explained in Sec. II.B. For "real" HO tracking data presented here, however, no ground truth is available, and these biases cannot be computed.

D. Subjective, HO Adaptation Detection Accuracy, and Lag

Figures 7c and 8c show the median of the button push times for each subject and will be analyzed from a performance and detection lag perspective. All HO button push results are listed in Table 3, according to their correctness for each respective condition, and are summarized in Table 4. Note that the time-invariant conditions TV1 and TV2 have no TP and FP (as never a change occurs) and should ideally only have TNs. The time-variant conditions TV12S and TV12F had no TN (as always a change occurs) and should ideally only have TPs.

The FPs were mainly incorrect pushes for the time-invariant conditions (15 for TI vs 5 for TV), with a majority in the TI2 condition

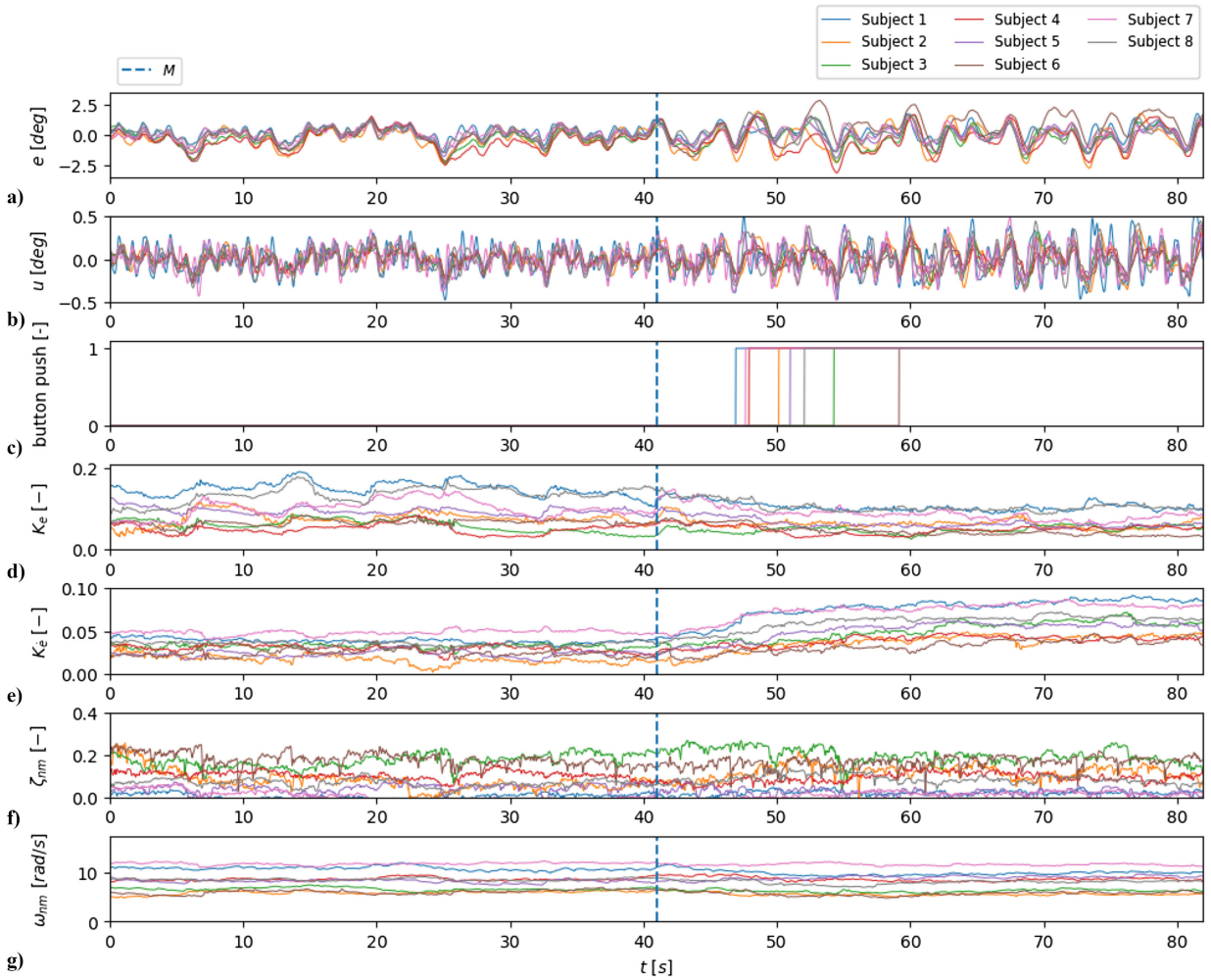

Fig. 8 Averaged time traces of control error a) and input b), median of button pushes c), and averaged time traces of identified HO parameters d–g) (all nine TV12S runs, per subject).

Table 3 Analysis of all HO button pushes (all subjects, all conditions).

Condition	TI1		TI2		TV12S			TV12F		
Result	FP	TN	FP	TN	TP	FN	FP	TP	FN	FP
Subject 1	0	3	0	3	9	0	0	9	0	0
2[a]	0	3	1	2	6[a]	2[a]	0[a]	7	2	0
3	0	3	3	0	7	1	1	8	1	0
4	3	0	3	0	7	0	2	6	2	1
5	0	3	2	1	7	1	1	9	0	0
6[a]	0	3	1[a]	1[a]	9	0	0	8	1	0
7	0	3	1	2	8	1	0	9	0	0
8	0	3	1	2	8	1	0	9	0	0
totals	3	21	12	11	61	6	4	65	6	1

[a]One run discarded for subjects 2 and 6.

Table 4 Summary of all HO button pushes, including the detection accuracy.

CondiKon, result	TP	TN	FP	FN	sum	Acc, %
TI conditions	— —	32	15	— —	47	68
W/o subject 4	— —	32	9	— —	41	78
TV conditions	126	— —	5	12	143	88
all conditions	126	32	20	12	190	83

(12). Here, the more difficult double-integrator-like dynamics may have confused subjects in detecting a changed CE. After debriefing, subject 4 indicated to be unaware of the option to *not* push the button during a run, resulting in six of the recorded FPs (3 in TI1, 3 in TI2); see Table 3. When subjects made a detection mistake, they often immediately told the experimenter (not shown). The accuracy in the TI runs was 68% (without subject 4, 78%).

FNs (12 in total) were spread among subjects and were equally spread over the TV12S (6) and TV12F (6) conditions, and thus no direct effect was found of G. The detection accuracy, as defined in Eq. (16), of the HO was 83% for all conditions (158/190), 88% when considering only the time-varying conditions (126/143).

By comparing the button push time with the moment of transition M, detection lags can be calculated. Their distribution for all subjects is shown in Fig. 9 for both time-varying conditions. Condition TV12F had a lower median detection lag (median 5.2 s) than TV12S (median 11.4 s). A dependent t-test showed that this difference is indeed significant ($t(7) = -3.63$, $p < 0.05$). This supports hypothesis H.1, which stated that HOs detect a change earlier (about 6 s in our experiment) when the CE dynamics transition occurs instantaneously.

The lower detection lag for TV12F makes sense, as the CE transition completion time in TV12S is much longer (≈15 s) than for TV12F (≈0.35 s). The slow CE change does not provide the HO the same opportunity to detect the transition, which is confirmed when plotting the distribution of button pushes against the sigmoid completion percentage (Fig. 10): the vast majority of button pushes occurred in the final 5% of the sigmoid change.

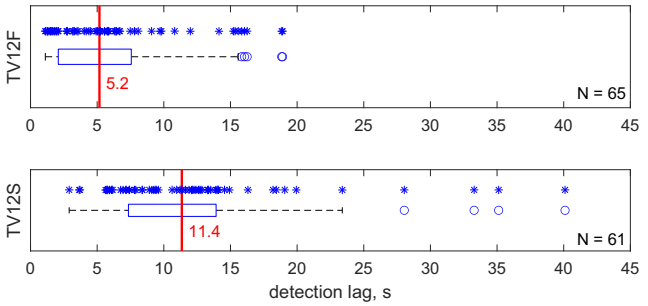

Fig. 9 Distribution of HO detection lags (all subjects, TV12F and TV12S conditions).

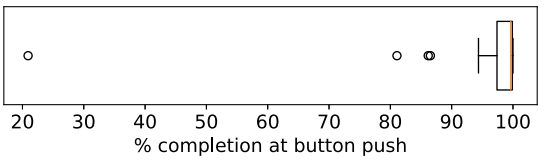

Fig. 10 Percentage of sigmoid transition completion required to trigger HO detection (TV12S).

E. Objective, TICA, and MA Adaptation Detection Accuracy

1. *Detection Procedure*

To illustrate the working principle of the two adaptation detection algorithms, typical example results for two different TV12F condition runs are shown in Figs. 11 and 12 for the TICA and MA methods, respectively. The initial hyperparameters for both methods ($\delta K_e = 0.06$, $\delta K_{\dot{e}} = 0.022$, $\Delta T = 3$ s, and for MA, $n_s = 1{,}500$) were heuristically based on visual inspection of the nature and variability of the estimated HO model parameter traces.

In these figures, three levels of the detection calculations are shown. First, the unfiltered detections are given, which are triggered whenever the estimated parameter trace (shown in red) is outside of the blue-shaded reference band (Figs. 11e and 12e). With the TICA example, the more variable K_e estimates lead to more false detections. Second, the detections that use the ΔT threshold are shown (Figs. 11f and 12f). Third, only the first occurrences of such detections are kept, resulting in the (blue) step signal of Figs. 11g and 12g. Per method, this filtering is performed for both the K_e and $K_{\dot{e}}$ parameter traces. In the MA example, Fig. 12, no detection was in the end found based on the K_e parameter trace since K_e never exceeded the reference band for longer than ΔT s, yielding an FN.

2. *Detection Accuracy Optimization*

Two hyperparameter tuning iterations were performed to obtain the best performance of the TICA and MA methods. Setting ($\delta K_e = 0.05$ and $\delta K_{\dot{e}} = 0.02$) and ($\delta K_e = 0.025$ and $\delta K_{\dot{e}} = 0.012$) for the TICA and MA methods, respectively, and ΔT and n_s unchanged, yielded a minimum MSE [Eq. (14)]. Table 5 shows the final results.

Both methods perform best using the ($K_{\dot{e}}$) parameter estimate trace, which was expected. When using this trace for detection, performance remains the same for both the rapidly changing (TV12F) and slowly changing (TV12S) CE condition. TICA performs best, with 57–58% accuracy, compared to MA, with 42–43% accuracy, when using the ($K_{\dot{e}}$) trace. The MA method has ≈9% more FPs and ≈6% more FNs than TICA.

F. Comparing Subjective and Objective Detection Lags

With the objective detection methods optimized, their performance in terms of timing (i.e., the moment a detection is made) can be compared with the subjective HO detection.[¶] Figure 13 shows the distribution of detection lags for all TP cases of the subjective HO detection (top, with some outliers not shown in the TV12S condition) and the MA and TICA detection methods. For the latter, only the $K_{\dot{e}}$-trace input cases are shown, as these yield the most TPs. In the MA and TICA figures, the thick gray vertical line shows the HO detection time median for ease of comparison.

To check the significance of the comparison, independent Welch's t-tests were used. This test can deal with different sample sizes in the compared groups. This is required because the number of runs in each boxplot is not the same, since only runs with a TP detection for the subjective and objective detection methods are included. Furthermore, the test should be independent since a TP HO detection and a TP detection by one of the methods are independent events.

In the TV12F condition, median detection lags are in the same order of magnitude (around 5 s) for both HO and the algorithmic methods. Differences between the HO and the TICA method

[¶]Note that the FP definition for the methods is stricter than for the subjective HO adaptation detection, as the former detection must be within 20 s (see Sec. II.C.2).

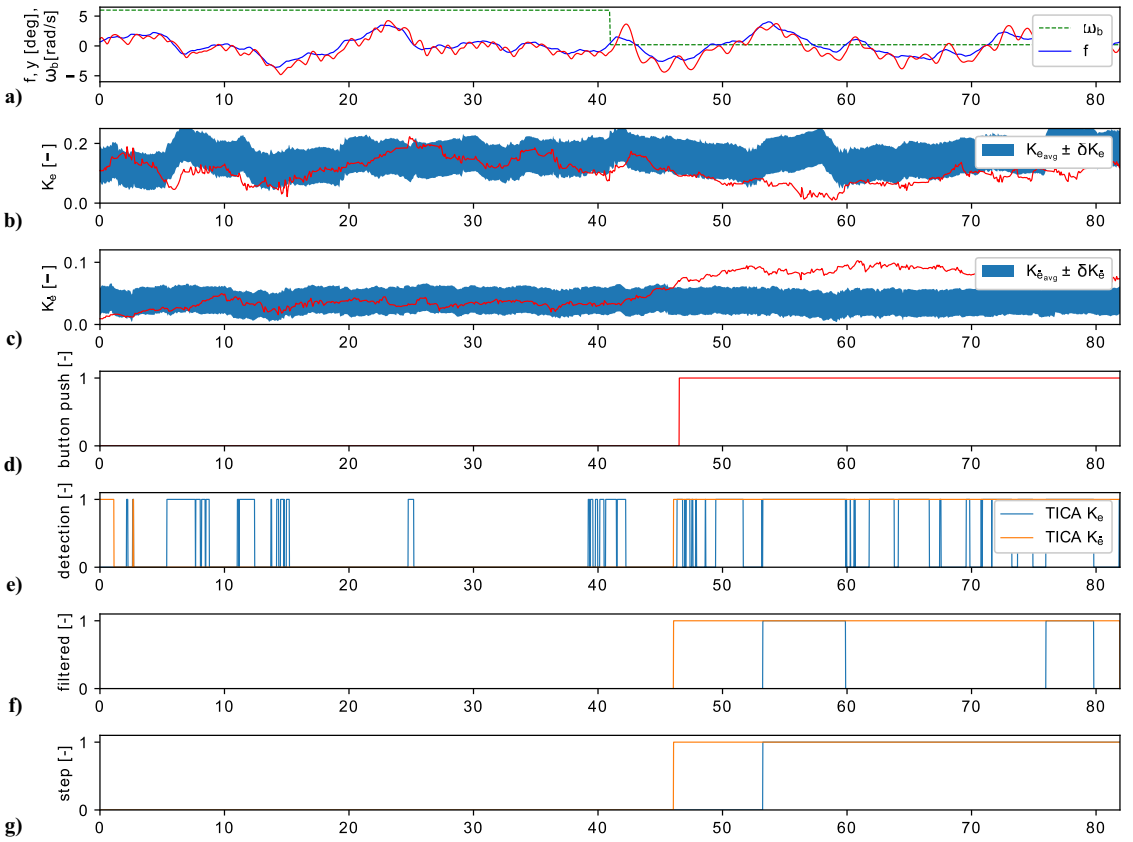

Fig. 11 Adaptation detection traces using TICA.

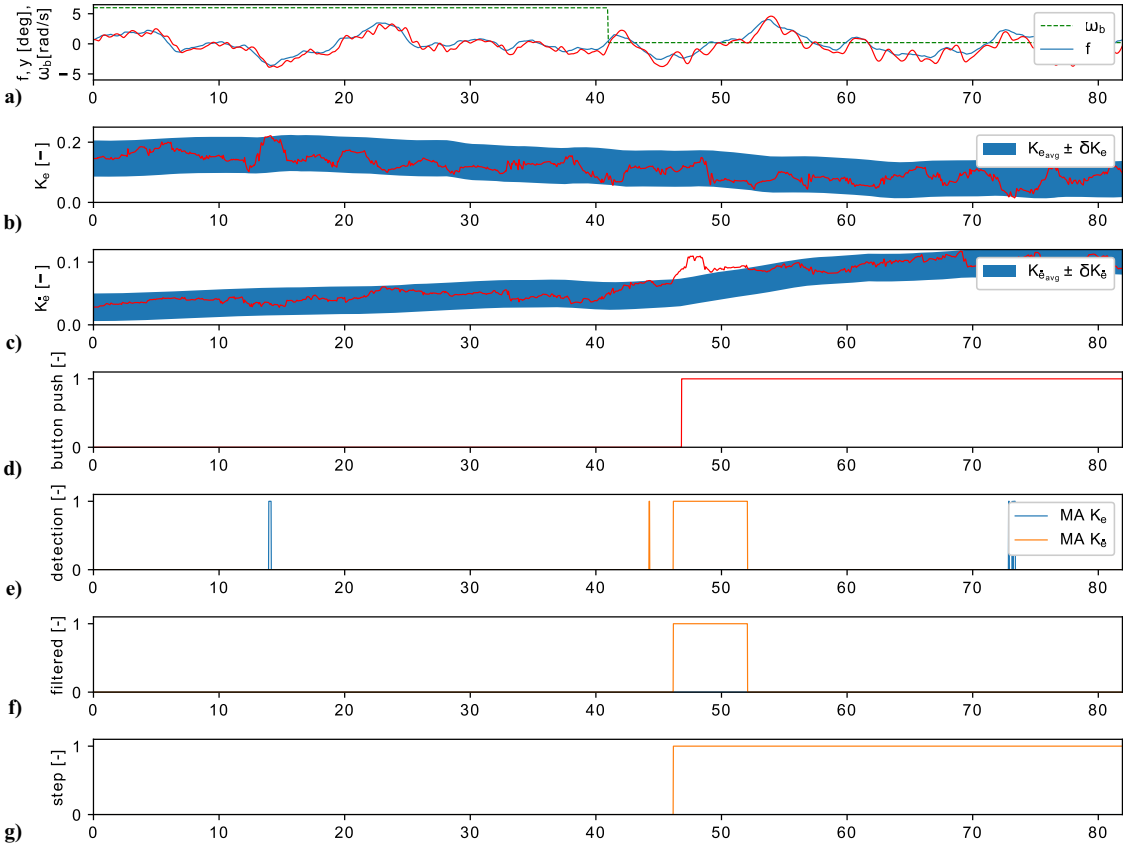

Fig. 12 Adaptation detection traces using MA.

Table 5 Detection accuracy, TICA, and MA methods (time-varying conditions only).

Condition	Method	Parameter	TP	FP	FN	sum	Acc, %
TV12F	TICA	K_e	16	41	15	72	22
		$K_{\dot{e}}$	41	24	7	72	57
	MA	K_e	9	50	13	72	12
		$K_{\dot{e}}$	31	30	11	72	43
TV12S	TICA	K_e	11	36	24	71	15
		$K_{\dot{e}}$	41	22	8	71	58
	MA	K_e	9	48	14	71	13
		$K_{\dot{e}}$	30	29	12	71	42

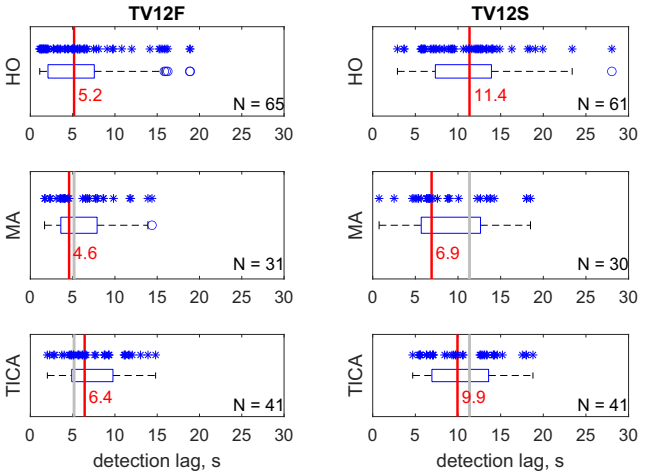

Fig. 13 Detection lags of TP detection of the HO and optimized TICA and MA methods (all subjects).

($t(103.1) = -1.62$, $p > 0.05$) and between the HO and the MA method ($t(79.4) = 0.0016$, $p > 0.05$) are not significant.

In the TV12S condition, both objective methods outperform the HO in how quickly they detect the adaptation when taking the median as the central measure. That is, they detect the HO adaptation *earlier* than the HOs' button presses: the MA method is approximately 4.4 s faster (a significant effect: $t(83.2) = 2.68$, $p < 0.05$); the TICA method is approximately 1.4 s faster (not significant $t(97.0) = 1.42$, $p > 0.05$).

It can be concluded that TICA is more accurate, but consistently later, than MA in its detection. Humans are more accurate but slower in their detection of the more gradual changing dynamics ($G = 0.5$ s^{-1}). For fast-changing dynamics ($G = 100$ s^{-1}), the HO has superior performance accuracy while being just a fraction slower than the objective methods. Note that in this setup, whereas the HO indicates a change in either perceived changes in the CE dynamics or in his/her adaptation to these changes, the objective method detects a change in the estimated HO dynamics alone.

V. Discussion and Recommendations

The feasibility of online human control model identification and adaptation detection is investigated using recursive ARX model identification. An experiment was performed where the CE dynamics were either single-integrator-like, double-integrator-like, or changed from the former to the latter at some unpredictable moment during the compensatory tracking run. Subjective data on *when the participant detected the dynamics transition* were obtained. The estimated time-varying HO control behavior parameter traces were used by two algorithms to objectively *detect when the operator starts adapting*. The dynamics transition occurred fast or slow, and our main hypothesis was that both subjective and objective detections were earlier and more accurate for faster transitions.

A. Online, Time-Varying HO Identification

Recursive ARX is indeed a feasible *online* identification method for time-varying HO dynamics, extending earlier work [26] to real-time applications. To the best of our knowledge, for the first time, HO parameter variations were estimated online and are shown as a function of time. The operator's equalization parameters (error gain K_e, error-rate gain $K_{\dot{e}}$, with the latter representing the operator *lead*) and neuromuscular limitations (natural frequency ω_{nm}, damping ζ_{nm}) were found to vary as expected: when transitioning from single-integrator-like to double-integrator-like dynamics, the error-rate gain significantly increased, requiring to maintain a stable control system.

The time delay in the HO model was fixed to 0.28 s, which showed to be close to the delays identified in the time-invariant k/s-like (average 0.29 s) and k/s^2-like (0.31 s) conditions. In contrast to McRuer and Jex [1967], who found an increase of 150 ms when comparing the time delay between their *pure* integrator and double-integrator dynamics, our results confirm those of Zaal [2016]. Tentatively, the fact that in our experiments pilots were found to generate lead in *both* conditions led to approximately the same time delays.

Results are promising, but significant steps still need to be made. First, the current method yields estimates of parameters of a simple model aiming to capture human behavior, and while these estimates are obtained in real time we have no "ground truth" to verify whether the estimates are correct. This fundamental problem exists, however, for *all* identification techniques applied to experimental HO data. Biases can only be investigated using *computer simulations* of a known, simulated, time-varying HO *model* [26]. Second, the HO time delay cannot be identified online, since in ARX models the delay parameter (shift n_k) cannot be included in the RLS update. Future work focuses on obtaining an estimate of the HO time delay in real time, for instance, using an approach where multiple ARX models with different n_k values are identified at the same time and evaluating which model captures the observed HO behavior best.

B. Objective Adaptation Detection

Two algorithms were developed to detect HO adaptation using the estimated time traces of either the HO model error gain K_e or the error-rate gain $K_{\dot{e}}$. While TICA created a fixed band of average gains based on *a priori* time-invariant data, the MA method used a running average of current gain estimates. Adaptation was considered "detected" when the current estimate of the gain was outside this fixed (TICA) or slowly changing (MA) band for 3 s, with the latter based on a hyperparameter optimization. Both methods showed the best performance when operating on the error-rate gain $K_{\dot{e}}$, the parameter trace showing the largest changes after transition, as mentioned above. Hence, our work clearly indicates that one should aim to capture the HO parameters that are the most likely to change, and to a significant extent (in magnitude), to become observable from the tracking data.

Both algorithms required hyperparameter tuning and did not achieve a level of accuracy that directly enables practical applications. Tentatively, the HO is more variable and noisy than generally assumed in our time-invariant modeling efforts. Analyzing the data run by run showed, for instance, that some subjects did not track the forcing function very well during some parts of the run, causing the HO parameter estimates to move outside the reference band quickly while the CE dynamics were the same. Tentatively, the algorithms were successful in detecting (intervals of) operator performance degradation, but were penalized in our approach as it focused on behavioral changes induced by a change in CE dynamics. Inherent fluctuations in the operator estimates were less consistent than expected, leading to a considerable number of FPs or FPs, impairing the algorithms' performance.

The MA method has three advantages over TICA, as it uses a past window of the *current* identified parameter trace for change detection: i) no prior measurements are needed, ii) it can be used online, and iii) it has no prior assumptions and continues to detect HO adaptation to different changes in CE dynamics. A disadvantage of both methods is that an interval of data is needed (here 3 s) to avoid too many FPs, causing detection delay.

Possible avenues to improve on these results could be to simulate and test with (transitioning or constant) pure SI to pure DI dynamics,

as in the current experiment subjects may have *also* applied considerable lead in the single-integrator-like condition ($T_L \approx 1/6 = 0.17$ s). Both detection algorithms only consider one of the four possible parameters, and it is worthwhile to pursue methods that use them all at the same time. Methods could be further improved by performing more extensive hyperparameter tuning, including a training/validation data split. Although tuning per subject could be warranted for certain applications to improve detection accuracy, this requires much more data. Overall, we conclude that the current performance is not spectacular and several tuning issues remain.

As a final note, this paper discussed the hyperparameter tuning of the TICA and MA algorithms; both were only tested offline. However, with the tunings obtained, both algorithms can be applied online without further work.

C. Adaptation Detection Performance: Timing and Accuracy

Regarding the *timing* of the adaptation detection, our main hypothesis, that detection occurs faster when the CE dynamics transition fast (a high G-value), is confirmed for both the subjective and objective detections. Both objective algorithms yield the highest accuracy when applied to the error-rate gain parameter. When only considering the true positives, the MA method is always faster than TICA and subjective HO detection, especially for the slow-changing CE transition (6.9 s vs, respectively, 9.9 s and 11.4 s). In the fast-changing CE transition, the HO detection (5.2 s) lies in between TICA (6.4 s) and MA (4.6 s). So when it comes to detection speed, the algorithms perform quite well and even detect operator adaptation *before* the operator detects the CE to change, especially when the dynamics transition occurs slowly. In fact, in the latter case, 95% of the HO detections occurred in the final 5% of the dynamics transition.

Regarding the *accuracy* of detection, the HO outperforms both algorithms in the time-varying runs (88% vs 57% (TICA) and 42% (MA)). The main reason for the lower accuracy of both algorithms is that they show many more FPs. For both the subjective and objective detections, there is no effect of fast or slow CE transitions on accuracy. This contradicts our main hypothesis, which stated that detection would be more accurate when the CE dynamics change rapidly. In contrast, the HO and TICA/MA detection accuracy is remarkably similar for the slow- and fast-changing CE transitions. Concluding, the TICA and MA methods do not match the detection qualities of the HO yet. When considering only the TPs, the latter methods could be sufficiently quick and accurate to detect HO adaptation to drive adaptive HO support systems. Whereas TICA is more accurate, the MA method achieves lower detection lags.

Note that, in our experiment, the participants were *instructed* to detect possible changes in the CE dynamics: they were aware, alert, and also *expected* a change to occur as this happened in the majority of conditions (75%). In more realistic situations, certainly in the case of actual operation, pilots are not aware, do not expect a change, and may react to such change in a different way. The two algorithms, on the other hand, do *not* depend on any expectations; they simply work on the estimated parameters that are fed to them. Comparing the algorithms' performance to the operator's performance in correctly detecting changes may therefore have been tilted in favor of the operator in the current experiment. The changes in operator behavior in real operation, reacting to an *unexpected* change in CE dynamics, may be larger and more easily identified by the algorithms. This is a topic of future work.

D. Further Research

The ARX-based identification method needs to be compared with other approaches reported in the literature [16,18,19,23–25], including estimates using neural networks [33,34]. Comparing the performance of methods, e.g., in terms of bias and variance of the obtained HO model parameters, can only be investigated through (massive) computer simulations. Special attention should be given to simulating representative HO remnant models and representative levels of HO nonlinearity and time-varying state. In this respect, as the authors of [26] and [29] have convincingly shown, the coupling of the HO dynamics and HO remnant model in the ARX model structure leads to biased parameter estimates. Therefore, other model structures, such as ARMAX or Box–Jenkins, which allow more degrees of freedom to resolve this coupling issue [32], must be investigated and made applicable in real time.

Second, all adaptation detection results presented in this paper could depend on the specific excitation caused by the single forcing function in the compensatory tracking task considered. Further research should investigate the effects of forcing function properties on time-varying HO adaptation and detection performance, bearing in mind that, in a realistic task, no similar excitation might happen.

Applying the developed methods to control tasks with a different kind of time-varying element could investigate the general usability of the adaptation detection methods. Compared to earlier work [6], the CE dynamics transition investigated in this paper (replicating Ref. [2]) was relatively benign. Better performance can be expected for more drastic transitions in CE dynamics (like a sign change [6]) requiring immediate and significant HO adaptation. From the perspective of actual operational use, however, picking up on more *subtle* changes (in the CE and operator dynamics, in the transition time) would be more relevant for the development of support systems. The current results show that indeed these slower changes require more time to detect than faster changes.

Perhaps more important would be to change the control task altogether and move to more relevant and realistic tasks with pursuit or preview displays. Not only is compensatory tracking an exception in real-life human control and not the rule [12], it can also be expected that human and algorithmic detection of adaptation will improve with a pursuit (or preview) display, as here the operator can directly *see* the result of one's control actions on the CE, whereas with a compensatory display these are not directly shown and have to be *inferred* from the error signal.

Possible applications for the adaptation detection methods are attention monitoring and adaptive HO support systems (e.g., haptic feedback [4]). Our current results show that, for these applications to work, a proper weighing will need to be found between reducing the amount of FPs or FNs, at the cost of TPs. Although hyperparameter tuning can be used to emphasize FP or FN suppression as much as possible, the severity of an erroneous detection in realistic settings will determine which classification errors should be reduced the most.

This paper shows that even in a simple, one-dimensional control task, where the pilot has one input and one output, automatically detecting HO behavior changes is challenging. Without adequately matched adaptations, the highly variable behavior of humans in realistic control conditions may severely hamper the potential of such adaptive systems, as any mismatched adaptations will quickly reduce an operator's trust in and acceptance of these systems. Given the variability in human behavior, even in simple tracking tasks, developing trustworthy, acceptable human–automation teaming systems seems a daunting challenge, requiring significant advancements in the state-of-the-art.

VI. Conclusions

The feasibility of online time-varying HO model parameter estimation using recursive ARX model fits has been demonstrated. Two methods to detect pilot adaptation using the recursively estimated operator model parameter traces, TICA and MA, were developed and tested. Data from a human-in-the-loop experiment with time-varying CE dynamics were used for validation. Results show that pilots (instructed to detect changes) correctly detected 88% of dynamics changes when they occurred. The objective detection methods were less accurate, 58% at best. When only considering the correct detection of pilots and algorithms, results show that for gradual CE dynamics changes, the MA method detects pilot adaptations approximately 4.5 s earlier than pilots do (6.9 s vs 11.4 s). For the fast dynamics transition, the detection lags of algorithms and pilots are similar (≈4.6–6.4 s). The observed variability in pilot control behavior, even in a simple one-dimensional compensatory tracking task, leads to a consistently high number of FPs of the detection algorithms. Developing adaptive pilot support and monitoring systems for more realistic manual control tasks require significant advancements in the state-of-the-art.

References

[1] Hess, R. A., "Modeling Pilot Control Behavior with Sudden Changes in Vehicle Dynamics," *Journal of Aircraft*, Vol. 46, No. 5, 2009, pp. 1584–1592.
https://doi.org/10.2514/1.41215

[2] Zaal, P. M. T., "Manual Control Adaptation to Changing Vehicle Dynamics in Roll-Pitch Control Tasks," *Journal of Guidance, Control, and Dynamics*, Vol. 39, No. 5, 2016, pp. 1046–1058.
https://doi.org/10.2514/1.G001592

[3] Farjadian, A. B., Annaswamy, A. M., and Woods, D. D., "Towards A Resilient Control Architecture: A Demonstration of Bumpless Re-Engagement Following an Anomaly in Flight Control," *Proceedings of the International Symposium on Sustainable Systems and Technologies*, Sustainability Conoscente Network, Phoenix, AZ, 2016, pp. 1–8.

[4] Van Baelen, D., Ellerbroek, J., Van Paassen, M. M., and Mulder, M., "Design of a Haptic Feedback System for Flight Envelope Protection," *Journal of Guidance, Control, and Dynamics*, Vol. 43, No. 4, 2020, pp. 700–714.
https://doi.org/10.2514/1.G004596

[5] Belcastro, C. M., Foster, J. V., Shah, G. H., Gregory, I. M., Cox, D. E., Crider, D. A., Groff, L., Newman, R. L., and Klyde, D. H., "Aircraft Loss of Control Problem Analysis and Research Towards a Holistic Solution," *Journal of Guidance, Control and Dynamics*, Vol. 40, No. 4, 2017, pp. 733–774.
https://doi.org/10.2514/1.G002815

[6] Young, L. R., "On Adaptive Manual Control," *Ergonomics*, Vol. 12, No. 4, 1969, pp. 635–674.
https://doi.org/10.1080/00140136908931083

[7] Mulder, M., Van Paassen, M. M., and Boer, E. R., "Exploring the Roles of Information in the Manual Control of Vehicular Locomotion: From Kinematics and Dynamics to Cybernetics," *PRESENCE: Tele-Operators and Virtual Environments*, Vol. 13, No. 5, 2004, pp. 535–548.
https://doi.org/10.1162/1054746042545256

[8] McRuer, D. T., and Jex, H. R., "A Review of Quasi-Linear Pilot Models," *IEEE Transactions on Human Factors in Electronics*, Vol. HFE-8, No. 3, 1967, pp. 231–249.
https://doi.org/10.1109/THFE.1967.234304

[9] Lone, M. M., and Cooke, A. K., "Review of Pilot Models Used in Aircraft Flight Dynamics," *Aerospace Science and Technology*, Vol. 34, April 2014, pp. 55–74.
https://doi.org/10.1016/j.ast.2014.02.003

[10] Xu, S., Tan, W., Efremov, A., Sun, L., and Qu, X., "Review of Control Models for Human Pilot Behavior," *Annual Reviews in Control*, Vol. 44, Oct. 2017, pp. 274–291.
https://doi.org/10.1016/j.arcontrol.2017.09.009

[11] Hess, R. A., "Structural Model of the Adaptive Human Pilot," *Journal of Guidance, Control, and Dynamics*, Vol. 3, No. 5, 1980, pp. 416–423.
https://doi.org/10.2514/3.56015

[12] Mulder, M., Pool, D. M., Abbink, D. A., Boer, E. R., Zaal, P. M. T., Drop, F. M., van der El, K., and van Paassen, M. M., "Manual Control Cybernetics: State-of-the-Art and Current Trends," *IEEE Transactions on Human-Machine Systems*, Vol. 48, No. 5, 2018, pp. 468–485.
https://doi.org/10.1109/THMS.2017.2761342

[13] Bachelder, E., and Aponso, B. L., "Human Pilot Control Adaptation: A Physiological Interpretation," *AIAA SciTech Forum*, AIAA Paper 2022-2446, Jan. 2022.
https://doi.org/10.2514/6.2022-2446

[14] Ameyoe, A., Chevrel, P., Le-Carpentier, E., Mars, F., and Illy, H., "Identification of a Linear Parameter Varying Driver Model for the Detection of Distraction," *Proceedings of the 1st IFAC Workshop on Linear Parameter Varying Systems*, Vol. 48, No. 26, 2015, pp. 37–42.
https://doi.org/10.1016/j.ifacol.2015.11.110

[15] Hess, R. A., "Modeling Human Pilot Adaptation to Flight Control Anomalies and Changing Task Demands," *Journal of Guidance, Control, and Dynamics*, Vol. 39, No. 3, 2016, pp. 655–666.
https://doi.org/10.2514/1.G001303

[16] Boer, E. R., and Kenyon, R. V., "Estimation of Time-Varying Delay Time in Nonstationary Linear Systems: An Approach to Monitor Human Operator Adaptation in Manual Tracking Tasks," *IEEE Transactions on Systems, Man, and Cybernetics—Part A*, Vol. 28, No. 1, 1998, pp. 89–99.
https://doi.org/10.1109/3468.650325

[17] Zaal, P. M. T., and Pool, D. M., "Multimodal Pilot Behavior in Multi-Axis Tracking Tasks with Time-Varying Motion Cueing Gains," *Proceedings of the AIAA Modeling and Simulation Technologies Conference*, AIAA Paper 2014-0810, 2014.
https://doi.org/10.2514/6.2014-0810

[18] Olivari, M., Nieuwenhuizen, F. M., üBlthoff, H. H., and Pollini, L., "Identifying Time-Varying Neuromuscular System with a Recursive Least-Squares Algorithm: A Monte-Carlo Simulation Study," *Proceedings of the 2014 IEEE International Conference on Systems, Man, and Cybernetics*, Inst. of Electrical and Electronics Engineers, New York, 2014, pp. 3573–3578.
https://doi.org/10.1109/SMC.2015.535

[19] Thompson, P. M., Klyde, D. H., and Brenner, M. J., "Wavelet-Based Time-Varying Human Operator Models," *Proceedings of the AIAA Atmospheric Flight Mechanics Conference*, AIAA Paper 2001-4009, 2001.
https://doi.org/10.2514/6.2001-4009

[20] Duarte, R. F. M., Pool, D. M., van Paassen, M. M., and Mulder, M., "Experimental Scheduling Functions for Global LPV Human Controller Modeling," *IFAC-PaperOnLine*, Vol. 15, No. 1, July2017, pp. 15,853–15,858.
https://doi.org/10.1016/j.ifacol.2017.08.2329

[21] Zaal, P. M. T., and Sweet, B. T., "Estimation of Time-Varying Pilot Model Parameters," *Proceedings of the AIAA Modeling and Simulation Technologies Conference*, AIAA Paper 2011-6474, Aug.2011.
https://doi.org/10.2514/6.2011-6474

[22] Zaal, P. M. T., and Sweet, B. T., "Identification of Time-Varying Pilot Control Behavior in Multi-Axis Control Tasks," *Proceedings of the AIAA Modeling and Simulation Technologies Conference*, AIAA Paper 2011-6474, Aug.2012.
https://doi.org/10.2514/6.2011-6474

[23] Schiess, J. R., and Roland, V. R., "Kalman Filter Estimation of Human Pilot-Model Parameters," NASA-TN-D-8024, NASA Langley Research Center, Hampton (VA), Nov. 1975.

[24] Popovici, A., Zaal, P. M. T., and Pool, D. M., "Dual Extended Kalman Filter for the Identification of Time-Varying Human Manual Control Behavior," *Proceedings of the AIAA Modeling and Simulation Technologies Conference*, AIAA Paper 2017-3666, 2017.
https://doi.org/10.2514/6.2017-3666

[25] Rojer, J., Pool, D. M., Van Paassen, M. M., and Mulder, M., "UKF-Based Identification of Time-Varying Manual Control Behaviour," *IFAC-PapersOnLine*, Vol. 52, No. 19, 2019, pp. 109–114.
https://doi.org/10.1016/j.ifacol.2019.12.120

[26] van Grootheest, A., Pool, D. M., van Paassen, M. M., and Mulder, M., "Identification of Time-Varying Manual Control Adaptations with Recursive ARX Models," *Proceedings of the AIAA SCITECH Modeling and Simulation Technologies Conference*, AIAA Paper 2018-0118, 2018.
https://doi.org/10.2514/6.2018-0118

[27] Nieuwenhuizen, F. M., Zaal, P. M. T., Mulder, M., van Paassen, M. M., and Mulder, J. A., "Modeling Human Multichannel Perception and Control Using Linear Time-Invariant Models," *Journal of Guidance, Control, and Dynamics*, Vol. 31, No. 4, 2008, pp. 999–1013.
https://doi.org/10.2514/1.32307

[28] Roggenkaemper, N., Pool, D. M., Drop, F. M., Van Paassen, M. M., and Mulder, M., "Objective ARX Model Order Selection for Multi-Channel Human Operator Identification," *Proceedings of the AIAA AVIATION Modeling and Simulation Technologies Conference*, AIAA Paper 2016-4299, 2016.
https://doi.org/10.2514/6.2016-4299

[29] Plaetinck, W"Online Time-Varying Identification and Detection of Operator Adaptation with Recursive ARX," *M.Sc. Thesis, Faculty of Aerospace Engineering*, Delft Univ. of Technology, Delft, The Netherlands, 2018.

[30] Plaetinck, W., Pool, D. M., van Paassen, M. M., and Mulder, M., "Online Identification of Pilot Adaptation to Sudden Degradations in Vehicle Stability," *Proceedings 2nd IFAC Conference on Cyber-Physical Proceedings of Human-Systems, Miami (FL)*, Vol. 51, No. 34, 2019, pp. 347–352.
https://doi.org/10.1016/j.ifacol.2019.01.020

[31] McRuer, D. T., Magdaleno, R. E., and Moore, G. P.,"A Neuromuscular System Activation Model," *IEEE Transactions on Man-Machine Systems*, Vol. 9, No. 3, 1968, pp. 61–71.
https://doi.org/10.1109/TMMS.1968.300039

[32] Ljung, L., —*System IdentificationTheory for the User*, 2nd ed., Prentice Hall, Upper Saddle River, NJ, 1999f.
https://doi.org/10.1002/047134608X.W1046.pub2

[33] Jiao, J., Sun, L., Tan, W., Xu, S., and Liu, X., "Identifying Pilot Control Adaptations to Sudden Changes in Aircraft Dynamics," *Journal of Guidance, Control, and Dynamics*, Vol. 46, No. 7, 2023, pp. 1408–1415.
https://doi.org/10.2514/1.G007358

[34] Versteeg, R., Pool, D. M., and Mulder, M., "Classifying Human Manual Control Behaviour Using LSTM Recurrent Neural Networks," *IEEE Transactions on Human-Machine Systems*, Vol. 54, No. 1, 2024, pp. 89–99.
https://doi.org/10.1109/THMS.2023.3327145

M. Jones
Associate Editor